International Journal of Technology

http://ijtech.eng.ui.ac.id

Research Article

Overlapping in Wire-arc Directed Energy Deposition Using Rotating Electrode

Andrea Bimbi[1], Yuta Sugiyama[1], Masahiro Kawabata[1], Hiroyuki Sasahara[1*]

[1]Department of Mechanical Systems Engineering, Tokyo University of Agriculture and Technology 2-24-16 Naka-cho, Koganei-shi, Tokyo 184-8588, Japan

[*]Corresponding author: sasahara@cc.tuat.ac.jp; Tel.: +81 42-00388-7417

Abstract: Adoption of additive manufacturing has enabled the fabrication of high-performance components with complex geometries. Tungsten Inert Gas (TIG) welding technology has been introduced to enhance the mechanical properties of the final products; however, it presents significant limitations in terms of achievable geometries. The rotary TIG technology addresses these limitations by rotating the electrode around the vertically fed filler wire. A series of overlapping beads were deposited while varying the electrode position to investigate the influence of process parameters in cladding using Rotary TIG, and the molten pool behavior was analyzed through thermal monitoring and high-speed imaging. The results show that positioning the electrode on the side of the previously deposited bead leads to flatter surfaces, achieving a max peak-valley distance of 0.343mm, allowing RTIG to be used in a regular TIG configuration. Placing it on the opposite side improves process robustness, allowing deposition under more constrained conditions, such as the repair of worn or geometrically irregular surfaces. Activating electrode rotation reduced the required current intensity for deposition while further enhancing surface flatness compared to the fixed-electrode configuration, achieving a max peak-valley distance of just 0.16 mm. Additionally, thermal analysis revealed a shading effect in the working zone, which was previously theorized in the literature, with significant implications for the wire melting dynamics.

Keywords: Cladding; Gas Tungsten Arc Welding; Rotary Tungsten Inert Gas; Wire-Arc Additive Manufacturing

1. Introduction

Additive Manufacturing (AM) has emerged as a groundbreaking technology, revolutionizing the manufacturing sector by enabling the production of highly intricate, custom parts with minimal waste (Tang et al., 2024; Pratheesh-Kumar et al., 2021). This method uses a diverse range of materials, including solid and liquid metals and polymers, allowing for flexible design and production. AM has seen rapid advancements in various industrial sectors in recent years, driven by its ability to create complex geometries that would be impossible or highly cost-prohibitive with traditional manufacturing methods (Vafadar et al., 2021; Cheepu et al., 2020; S. H. Huang et al., 2013).

One of the key areas of growth in AM is in metal manufacturing processes through the Directed Energy Deposition (DED), where welding technologies such as Metal Inert Gas (MIG), Tungsten Inert Gas (TIG), and Gas Plasma Welding (PAW) have been integrated into these systems (Nahmany and Aghion, 2025; Zhang et al., 2024; Shah et al., 2023; Li et al., 2022; Sahoo and Tripathy, 2019; Wu et al., 2018)). Wire Arc Additive Manufacturing (WAAM), which utilizes wire-fed DED techniques, has gained widespread attention. The advantages of WAAM include high efficiency, applicability to medium and large-scale parts, relatively low material and equipment costs, material waste reduction of up to 60% (Campatelli et al., 2020), and subtractive machining. In WAAM, metal is deposited through an electric arc that melts

https://doi.org/10.14716/ijtech.v17i1.8224
Received June 2025; Revised November 2025; Accepted November 2025

and deposits welding wire layer by layer, which can be done on both flat and complex surfaces. MIG and TIG are two primary welding methods employed in WAAM. MIG welding, also known as Gas Metal Arc Welding (GMAW), uses a consumable wire electrode with a shielding gas, usually pure argon or a blend with carbon dioxide, forming the necessary arc to melt the wire and fuse it to the workpiece. MIG welding is particularly favored for its speed and efficiency, making it ideal for relatively high-volume industrial applications. Recent innovations in MIG, such as Cold Metal Transfer (CMT), have further improved the process by reducing the thermal input, minimizing residual stresses, and achieving more precise welds with better shape accuracy (Karim et al., 2024; Wang et al., 2020a; Selvi et al., 2018). On the other hand, TIG welding, also known as Gas Tungsten Arc Welding (GTAW), operates with a non-consumable tungsten electrode, which, unlike MIG, does not melt, generating a stable arc. Instead, the welding wire is added separately from the side of the welding arc, allowing for more precise control over the welding process (Wang et al., 2020a). TIG welding is known for its ability to produce clean, high-quality welds with minimal spatter, making it ideal for applications, such as in aerospace, medical devices, and other high-quality requirements industries (Xiong et al., 2020; Bonaccorso et al., 2011). TIG is especially advantageous when producing welds with superior mechanical properties, as it results in stronger, more fatigue-resistant, lower joints porosity, superficial roughness, and undercutting (Ullah-Khan et al., 2024; Singh et al., 2022).

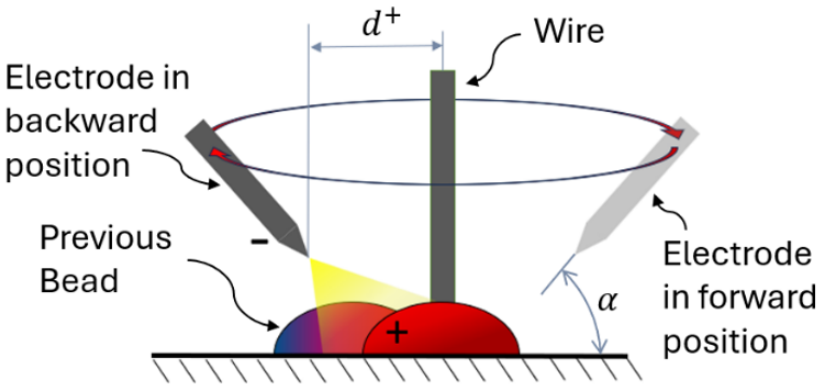

Figure 1 The rotary TIG overlapping process scheme

Despite the advantages of GMAW and GTAW, both methods face challenges, especially when used for AM. One of the main challenges with traditional TIG welding in AM is the deposition process's directional dependence. Since the wire is fed from the side, the deposition conditions can vary depending on the welding torch's travel direction. This directional dependence can cause inconsistencies in the weld bead, especially in complex geometries where the torch direction needs to change frequently (Kawabata et al., 2024b). To overcome this challenge, TAIYO NIPPON SANSO Corporation proposed rotary TIG welding. As shown in Figure 1, a rotating electrode that turns around a vertically fed wire is integrated. This rotation and the vertical feeder axis remove the directional dependence problem seen in traditional TIG welding. Rotary TIG welding has made it possible to produce high-quality, multi-layered structures, making it a suitable choice for fabricating intricate parts that require both precision and strength (Bimbi, Kawabata, Tsunekawa, Sasahara, and Campatelli, 2024; Kawabata et al., 2024b). With the development of the Rotary TIG, it becomes essential to explore the effects of the varying deposition parameters.

Given AM's inherent versatility in material deposition, evaluating how effectively each technology performs across different applications is essential to fully exploit its potential and enhance its industrial adaptability, as a single machine can be employed for multiple operations. AM is also widely used for repairing worn parts and creating cladded surfaces (W. Huang et al., 2024; Xu et al., 2024; Sarkar et al., 2022; Yin et al., 2018); however, the behavior of rotary TIG is unknown. As a first step toward this direction, this study focuses on evaluating the quality of TIG-produced coatings in relation to specific welding. The melting pool is subjected to different

stresses according to the electrode edge and wire axis distance (d), which affects the final surface quality. Investigating the role of these aspects, including the impact of unique parameters such as the activation of electrode rotation, as well as the effect of using different fixed electrode positions during deposition when operating in a regular TIG configuration, is essential. The results demonstrate that rotary TIG can also be employed as a conventional TIG AM system with a vertically fed wire.

2. Methods

2.1 Set up

The first approach of the research activity concerned the understanding of which geometric model fits the single beads made using rotary TIG. Using this new technology, it has been necessary to choose the correct model for the overlapping beads. Some geometrical models exist (Baffa et al., 2022; Chen et al., 2022; Han et al., 2021; Li et al., 2018; Ding et al., 2015) that do not depend on the deposition technology but on the best fitting shape of the single beads. Since this technology also allows to change the distance between the electrode edge and the wire center d, it has been selected as 3 mm, 4 mm, and 5 mm (Figure 1). As shown in Figure 1, when the wire touches the melting pool, it becomes part of the positive pole. Therefore, with a fixed electrode inclination of α= 60° with respect to the torch axis, if d was lower than 3 mm, the electric arc would strike between the electrode edge and the wire feeder. Over 5 mm, the arc would not have involved the wire, effectively not melting it. Plastic jigs have been 3D-printed and used to ensure the correct electrode holder positioning, one for each desired distance. Since the distance between the electrode vertex and the base plate heavily affects the heat input (Kawabata et al., 2024a; Kawabata et al., 2024b), it was fixed at h_0 = 5 mm. The distance between the bottom surface of the rotor and the electrode edge was h_1= 8 mm. ∅ 3.1 mm diameter WIG Elektroden WLa20 tungsten electrodes. Since the shape of the top of the electrode affects the arc properties (Abid et al., 2013), a β= 50° conic top was selected for all the experiments. The gas flow was 20 L/min for both the coaxial ducts for 40 L/min. Since this is the first rotary TIG overlapping study, the selected material was stainless steel JIS G4304 SUS304 for both the 150 x 150 x 5 mm base plates and for the ∅ 1.2 mm wire (Table 1). The torch body was connected to the Daihen PU-301 Watertank heat exchanger, while the external cooling collar and the base plate were connected in series to the Daihen PU-701Watertank heat exchanger. The experiments were conducted with the assistance of a 4-axis computerized numerical control machine (Mutoh Value Arc MA5000-S1).

Table 1 Composition of wire and base plates

Material Name	C	S	P	Si	Mn	Ni	Cr	Fe
JISG4304SUS304	≤0.08	≤0.030	≤0.045	≤1.00	≤2.00	8.00–10.50	18.00–20.0	Bal.

Quantities are expressed as weight percentages

Tanaka TIG Sanark Meister provided the WFS value. Except for the current intensity and the WFS, all system parameters and inputs were defined using Artsoft Mach 3 Mill software via G-Code. The overlapping process was monitored using a regular camera, a high-speed camera (HS cam), and a thermal camera. The first one could highlight the final shape of the coating, and the second one could highlight the shape of the melting pool. To conduct analyses, it is necessary to remove the electric arc light by exploiting a band pass filter. The working area was illuminated using an ultraviolet light source compatible with the filter. With reference to the wire, the light source was positioned on the opposite side of the camera to highlight the shape of the molten pool by generating shadowed areas.

2.2 Single Beads

The electrode can rotate or be positioned in a fixed orientation: since the superficial quality of the weld beads using low rotational speeds is very rough and the internal structure is irregular (Bimbi, Kawabata, Tsunekawa, and Sasahara, 2024; Kawabata et al., 2024b), a rotational speed of 500 rpm was selected. The beads were then deposited, and the electrode was fixed on one side, forward, and backward of the torch center. The rotation direction affects the arc trajectory, allowing it to give more energy to one side of the torch trajectory than to the other. However, the trajectory shape is symmetric at 500 rpm; thus, only the clockwise direction has been arbitrarily chosen. Welded beads of length 55 mm were successfully deposited by selecting 150 and 200 A as current intensities, a wire feed speed (WFS) of 1 m/min, and a torch travel speed (TS) of 200 mm/min. Because WFS and TS were fixed, the speed ratio (SR) shown in Eq. 1 was also fixed to 5.

$$SR = \frac{WFS}{TS} \tag{1}$$

The beads were scanned using an optical 3D scanner (Keyence VL 300 Structured Light Scanner), which provided point clouds for merging. Keyence VL 300 3D scanner native software (VL Series Application) was used to analyze the welded beads. Twelve cloud points were acquired for each weld bead and then superimposed by rotating the plate with the deposited material by 30° after each acquisition using the scanner's rotation mechanism for a total of 360°. The points of five parallel sections were sampled for each weld bead. The first scanned section was taken at 20 mm from the beginning of the weld bead to avoid the thermal transient affected portions, and the others were 2 mm from each other. Several geometrical models have been developed to calculate the best step over value d* for the overlapping of beads (Chen et al., 2022; Han et al., 2021; Li et al., 2018; Ding et al., 2015). According to the best fit shape a model for the d* value: parabola Eq. 2, cosine arc Eq. 3, Eq. 4, and an exponential curve Eq. 5. As explained by Han et al., 2021, the exponential parameter t is the only value that affects the plumpness coefficient k of the exponential model in Eq. 6. For the circular-arc model, k depends on a function of a and b, whereas for the parabola and cosine arc models, the plumpness values are constants, 0.667 and 0.637, respectively.

$$y = ax^2 + b \tag{1}$$

$$y = a \cdot \cos(bx) \tag{2}$$

$$y = \sqrt{a^2 - x^2 + b} \tag{3}$$

$$y = |x|^t + b, \quad a < 0,\ b > 0,\ t > 1 \tag{4}$$

$$k = \frac{t}{1+t} \tag{5}$$

In the results and discussion section, it is shown that the best-fitting models for the rotary TIG single-bead sections are the exponential and the parabola ones, even if the latter cannot adapt its own plumpness to the real section shape. To obtain the most regular surface by overlapping, the optimal step over must be determined. According to the Tangent Overlapping Model (*TOM*) proposed by Ding et al. (Ding et al., 2015), if the best fitting is a parabola, can be calculated using Eq. Eq 7. and according to Exponential *TOM (TOMexp)* proposed by Han et al., 2021, if the best fitting model is the exponentcan be calculated usingculate it by Eq. 8. w is the width of the single bead and *f(t)* is a complex function of the exponential parameter t, a script has been developed to calculate it according to the data presented by Han et al., 2021 in their work.

$$d^* = 0.738\, w \tag{6}$$

$$d^* = f(t)\, w \tag{7}$$

To avoid overlapping defects and validate the exponential method, the plumpness value was checked to be higher than 0.637 (cosine curve k value) and lower than 0.700 (Han et al., 2021). The average energy consumption is also given in the same table, calculated according to Eq. 9 (Kawabata et al., 2024b; Carvalho et al., 2023; Baffa et al., 2022), where r is the metal wire radius. A Matlab script has been developed to extract all the parameters of interest.

$$e = \frac{60 \cdot I \cdot V}{1000 \cdot WFS \cdot \pi r^2} \tag{8}$$

3. Results and Discussion

3.1 Single Beads

Twenty single beads were successfully deposited using rotary TIG and analyzed using a 3D scanner. The relevant results are summarized in Table 2. The best fitting data are shown: It is easy to see that the sections fit in all the proposed curves with a very high determination coefficient R^2, the highest values are underlined. However, confirming previous studies, the best fitting curves are the parabola and exponential ones. Considering the proposed system configuration and the arc rigidity, using an electrode edge to wire feeder axis distance of 5 mm, the arc axis will intersect the base plate at about 1.5 mm from the wire; therefore, the arc barely enveloped the wire. Assuming that the arc shape is gaussian shaped (Wang et al., 2020b; Dai et al., 2018b; Dai et al., 2018a), using a current intensity of 150 A with this setup, the wire did not melt properly and hit the bottom of the melt pool, creating incomplete weld beads. The most critical configuration was to position the electrode on one side. Apart from using a distance d = 3 mm (test no. 1), all the other 150 A deposited beads were complete, but their geometry was irregular. The plumpness value k was calculated for all sections. For the 200 A deposited weld beads, k values were in the range of 0.637 and 0.700, confirming that, where necessary, the TOM_exp model (Han et al., 2021) can also be applied to the rotary TIG. In the front fixed electrode cases, the arc slightly oscillated in the transversal direction, making the repeatability of the weld beads geometry difficult. Furthermore, the width slightly varied along the longitudinal direction. The rear positioning case was the worst case: the bead was slightly irregular. Therefore, the parameters of tests 1, 2, 4, 10, and 12 were selected to realize overlapping experiments.

Table 2 Parameters, geometry, best fitting data using parabolic, circular, cosine, and exponential fitting curves, and overlapping parameters of the single-bead experiment

Test	d(mm)	rpm	IA	VV	e(J/mm^3)	w(mm)	h(mm)	Par.R^2	Circ.R^2	Cos.R^2	Exp.R^2	t	k	$f(t)$	d^*(mm)
1	3	500	150	11.7	92	4,73	1,87	0.9902	0.9933	0.9884	0.9944	2,41	0,706	0,8001	3,491
2	3	500	200	12.2	128	9,06	1,01	0.9982	0.9989	0.9979	0.9995	2,19	0,686	0,7836	7,096
4	3	side	200	13.4	144	9,61	1,07	0.9951	0.9878	0.9892	0.9893	1,83	0,646	0,7126	7,093
10	4	500	200	13.6	144	9,38	1,04	0.9981	0.9955	0.9952	0.9953	2,025	0,669	0,8919	6,921
12	4	side	200	12.2	129	8,70	1,01	0.9938	0.9819	0.9807	0.9808	1,88	0,652	0,842	6,424

WFS = 1 m/min; TS = 200 mm/min; SR = 5; bead length = 55 mm; 20+20 L/min Argon; h_0 = 5 mm; h_1 = 8 mm; α = 30°; β = 50°; ∅ 3.1 mm electrode; ∅1.2 mm SUS304 wire; SUS304 base plate

3.2 Overlapping

Using the 12 test parameters, six beads have been regularly overlapped. As shown in Figures 6 a) and b), because the electrode is fixed on one side of the wire, the arc affects it from the same direction and non-homogeneously melts it. The heat input is homogeneously given by activating the rotation, and the wire melts before hitting the bottom of the pool. Thanks to this beneficial effect, it is possible to decrease the current intensity to 150 A. Figure 2 shows the obtained overlapped surfaces. The red dashed line indicates the section reference used to obtain the sections of Figure 3. In Figure 3 a), the maximum height step is approximately 0.28 mm. Using test 2 parameters and increasing the current to 200 A, spatter occurred, creating

beads with variable width and humping beads. The maximum valley-peak distance was about 0.85 mm using test 10 parameters. Figure 3 shows the cross sections of the realized coating surfaces. In Figure 3 b), the maximum height step was approximately 0.34 mm. Figures 3 a) and b) show how different the overlapped bead geometry is just by changing the electrode side. The electrode is positioned on the opposite side with respect to the already welded beads. The wire falls next to the previous bead, guaranteeing the continuity of the coat. It guarantees wider applicable conditions, making this set-up suitable for repairing or specific base plate shapes or conditions. Positioning the electrode on the same side of the previously welded beads ensures a smoother surface. To clarify these aspects, it was necessary to check the shape of the melting pool. If the electrode is fixed on the forward side, the wire position is on the previous deposited bead's edge. This positioning ensures continuous surface deposition because the material is fed closer to the already solidified one.

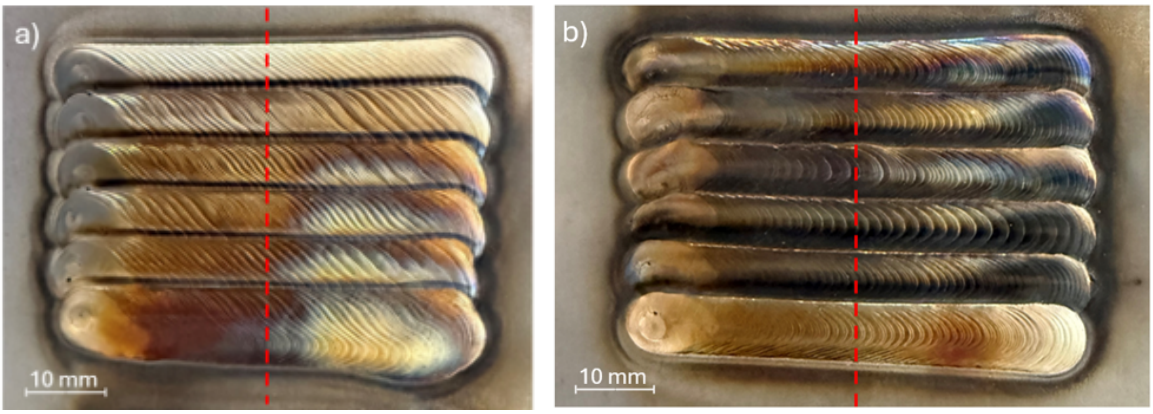

Figure 2 Figure 2 Cladded surfaces realized using 200 A, electrode tip - wire distance d = 4 mm and a) backward fixed electrode; b) forward fixed electrode

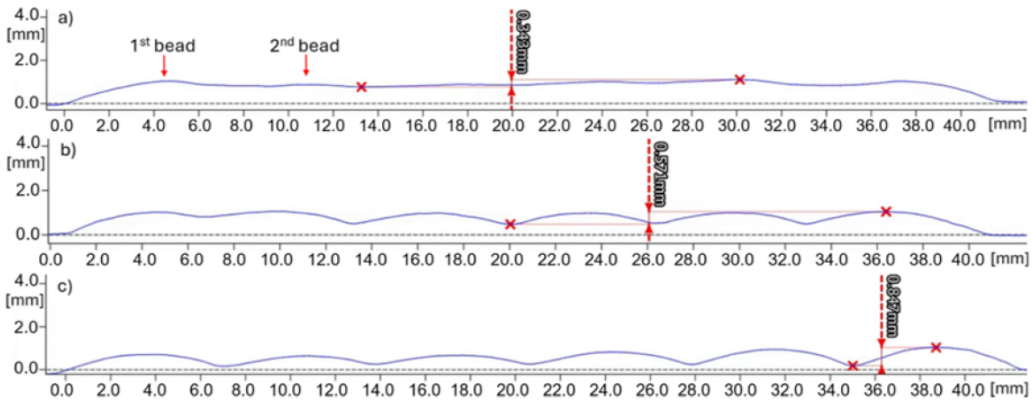

Figure 3 Figure 3 200 A, electrode tip - wire distance d = 4 mm and a) forward fixed electrode; b) backward fixed electrode; c) 500 rpm cladded samples cross-sections

However, if the electrode is fixed on the backward side, the arc gives more energy to the metal between the previously deposited bead and the wire. Owing to the lower viscosity and superficial tension of the material and the arc pressure, the fluid metal can flow and adjust itself in the available space. Figure 4 shows the overlapping process from a longitudinal perspective. Figures 4 c), d), and f show that it is possible to see a dark area in the middle of the metal pool. Since the light source is behind the wire, it is a shadow area, which means the arc pressure pushes the material of Figure 4 e). As shown in Figure 4 a) and c), this configuration creates a pool with an almost flat surface. As highlighted in Figure 4 b) and d), if the electrode is fixed on the forward side, the arc action is insufficient to adjust the melting pool shape; thus, its surface will create an angle with the previous welded bead. Furthermore, as shown in Figure 5a), the coating valleys are not in the middle of the adjacent beads; they are on the side of the

torch trajectory. To understand the reasons, another experiment was conducted, maintaining the same d* but increasing the current intensity to 225 A. Using these parameters, the material receives more energy and pressure, facilitating the fluid metal flow. As shown in Figure 5 b), the valleys became deeper, and their position still shifted from the torch trajectory. This is due to the increased arc pressure acting on the molten pool and not due to the lack of material feeding between the beads. Figure 4 f) highlights how the melting pool becomes wider and a step forms between two contiguous beads. It is also possible to notice how the melting pool surface level was lower than that of the base plate one: these conditions increase the material mixing. Thus, an optimal current intensity exists. According to the results of 150–225 A experiments, 200 A gives the flattest surface. Another experiment has been conducted exploiting the test no. 1 parameters, so electrode rotation. Since the current is low, the single beads are taller and narrower, resulting in a thicker coating and a longer working time required to cover a certain area. This configuration is preferable for smaller-area coatings reducing the energy cost. Furthermore, the arc rotates over the entire working surface, resulting in a second beneficial effect: a more uniform distribution of the molten material due to the homogenization of the pressure and heating distributions.

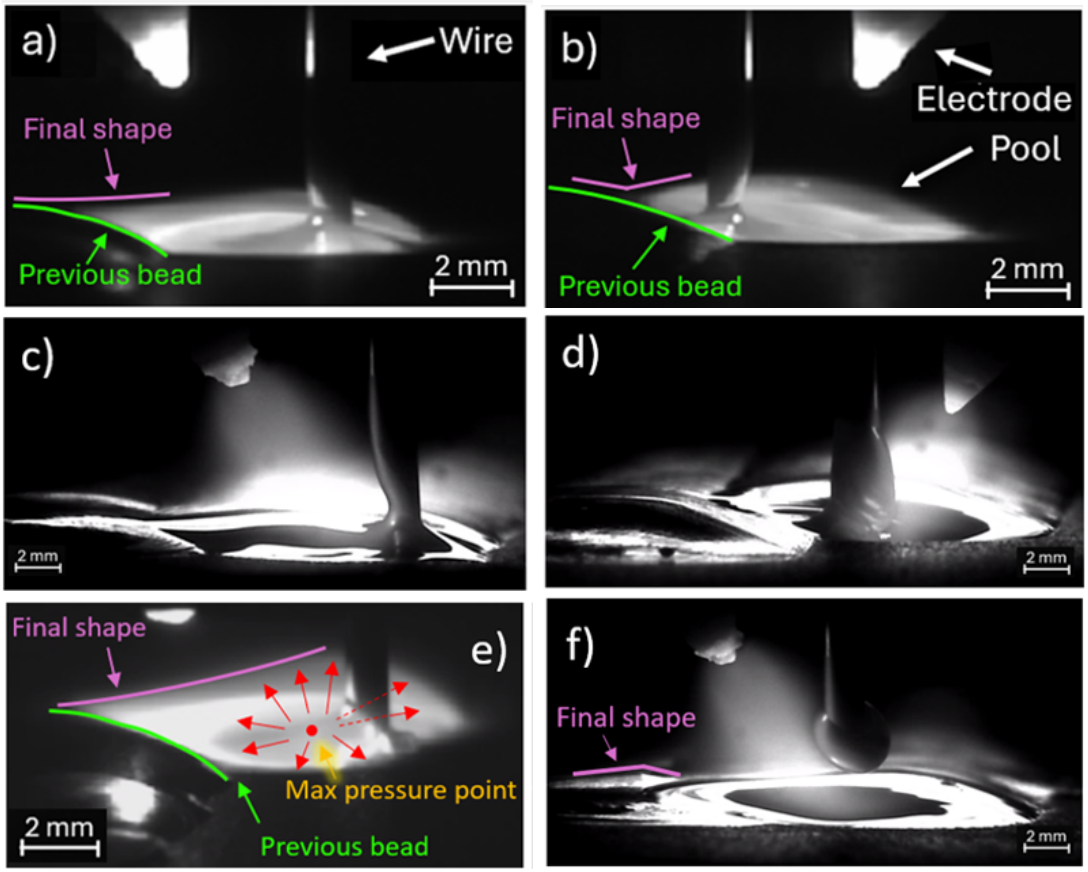

Figure 4 Overlapping process longitudinal perspective using a) backward, b) forward, c) backward (HS cam), d) forward (HS cam) fixed electrode. e) Pressure effect scheme, f) 225A process (HS cam)

As shown in Figure 7, it leads to the best surface quality, with a maximum valley-peak distance of only 0.16 mm. Enabling a reduction of the required current for depositioning down to 150 A, consequently decreases the overall heat input, an essential factor in limiting the thermal impact on the heat-affected zone, potentially improving the final product quality. The experiments were also monitored using a thermal camera. As shown in Figure 6, the electric arc does not fully envelop the filler wire, which casts a shadow on the workpiece surface. This shadow effect prevents the uniform melting of the wire.

This observation explains why it is possible to decrease the required current intensity by

activating the electrode rotation, thereby rotating the arc itself, which is the distinctive feature of Rotary TIG. By selecting 500 rpm, weld beads can be deposited using a lower current intensity without the wire tip penetrating the bottom of the molten pool. The shadow effect has already been theorized in previous studies (Bimbi, Kawabata, Tsunekawa, and Sasahara, 2024).

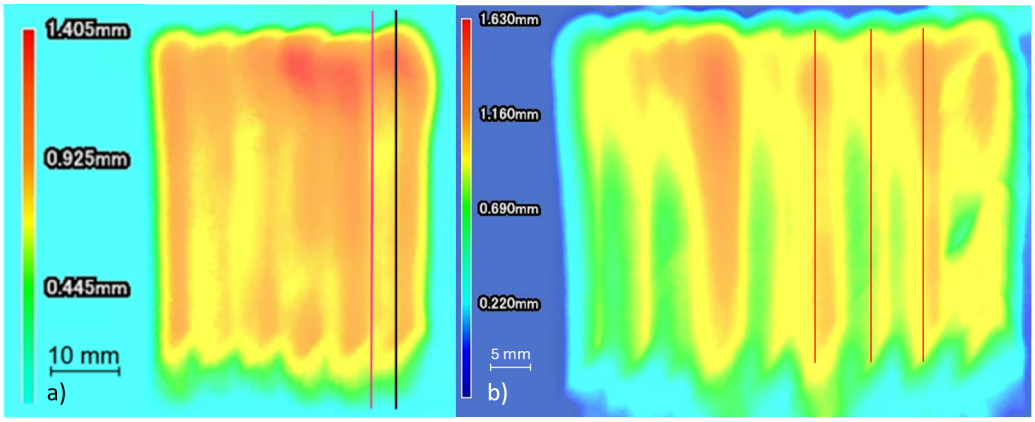

Figure 5 Coating surfaces using d = 4 mm, backward fixed electrode: a) 200A, b) 225A height analyses

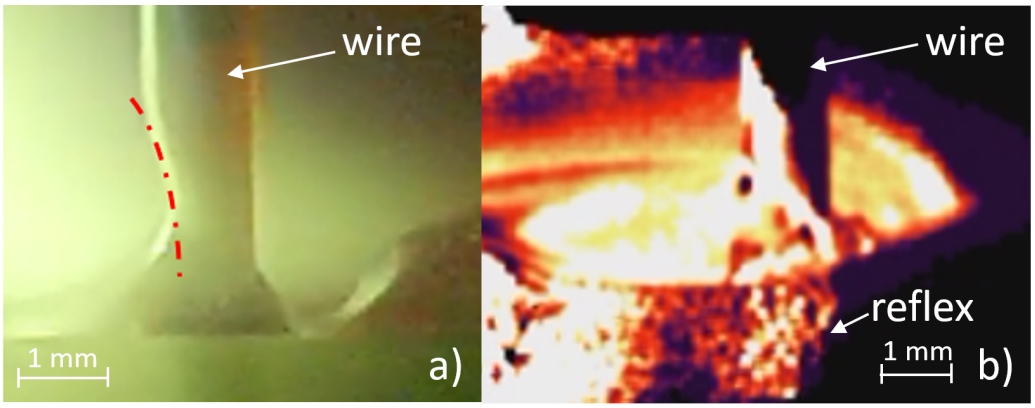

Figure 6 Overlapping process, longitudinal perspective using 225 A, backward fixed electrode, d = 4 mm, a) regular camera and b) thermal camera (colored = melted). Non-homogeneous wire melting

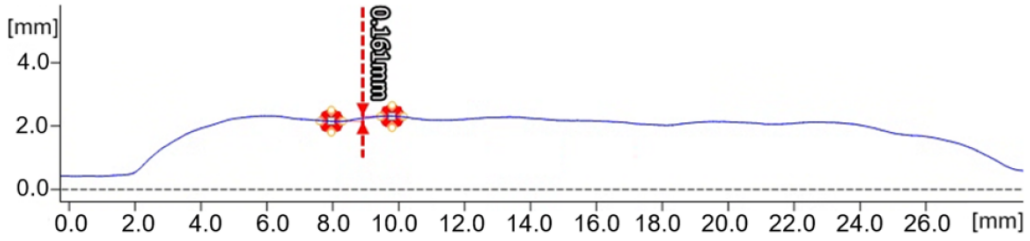

Figure 7 Cross sections of overlapped single beads using 200 A, 500 rpm, d = 3 mm

4. Conclusions

Twenty single beads were deposited to define the best parameters for the cladding process using rotary TIG. The coatings have been realized, and the results have been analyzed. The position of the electrode relative to the previous bead strongly affects coating quality: placing it on the backward side improves the continuity and enables deposition under more constrained conditions, whereas placing it on the forward side improves the superficial smoothness. This sensitivity can be exploited to adapt the process to specific production requirements. Using a

fixed electrode, a current of 200 A proved to be optimal, providing the flattest surface compared to incomplete deposition at 150 A and instability at 225 A. This is due to the arc pressure that changes according to the amperage, which affects the behavior of the melting pool. The maximum recorded surface peak-to-valley distance is only 0.343 mm, confirming that rotary TIG can also be effectively employed in a standard TIG configuration. Electrode rotation improved the flatness of the deposited surface, with a maximum peak-to-valley distance of just 0.16 mm. Thermal imaging revealed that activating electrode rotation promotes uniform melting of the filler wire, reducing the required current. This, in turn, lowers the heat input, which is critical for minimizing the impact on the base plate's heat-affected zone and increasing the final product quality.

Nomenclature

AM	Additive Manufacturing
DED	Directed Energy Deposition
GTAW	Gas Tungsten Arc Welding
HS cam	High Speed Camera
MIG	Metal Inert Gas
PAW	Gas Plasma Welding
SR	Speed Ratio
TIG	Tungsten Inert Gas
TOM	Tangent Overlapping Model
TOM_{exp}	Exponential TOM
TS	Torch Travel Speed
WAAM	Wire Arc Additive Manufacturing
WFS	Wire Feed Speed

Acknowledgements

TAIYO NIPPON SANSO Corporation provided valuable technical support during the research period. TOKYO UNIVERSITY OF AGRICULTURE AND TECHNOLOGY provided financial support and grant for 6 months through the FLOuRISH-SPRING's JST SPRING 2025 Grant no. JPMJSP2116. JUN KINOSHITA provided valuable support during the research by assisting with the operation of machinery at the production facilities of TOKYO UNIVERSITY OF AGRICULTURE AND TECHNOLOGY.

Author Contributions

Conceptualization, Andrea Bimbi, Yuta Sugiyama, Masahiro Kawabata, and Hiroyuki Sasahara; methodology, Andrea Bimbi, Yuta Sugiyama, Masahiro Kawabata, and Hiroyuki Sasahara; software, Andrea Bimbi and Yuta Sugiyama; validation, Masahiro Kawabata and Hiroyuki Sasahara; formal analysis, Andrea Bimbi; investigation, Andrea Bimbi and Yuta Sugiyama; resources, Hiroyuki Sasahara; data curation, Andrea Bimbi and Yuta Sugiyama; writing—original draft preparation, Andrea Bimbi; writing—review and editing, Andrea Bimbi, Masahiro Kawabata, and Hiroyuki Sasahara; visualization, Andrea Bimbi and Yuta Sugiyama; supervision, Masahiro Kawabata and Hiroyuki Sasahara; project administration, Andrea Bimbi and Hiroyuki Sasahara; funding acquisition, Andrea Bimbi and Hiroyuki Sasahara.

Conflict of Interest

The authors declare no conflicts of interest.

References

Abid, M., Parvez, S., & Nash, D. H. (2013). Effect of different electrode tip angles with tilted torch in stationary gas tungsten arc welding: A 3d simulation. *International Journal of Pressure Vessels and Piping*, *108–109*, 51–60. https://doi.org/10.1016/j.ijpvp.2013.04.006

Baffa, F., Venturini, G., Campatelli, G., & Galvanetto, E. (2022). Effect of stepover and torch tilting angle on a repair process using waam. *Advances in Manufacturing*, *10*(4), 541–555. https://doi.org/10.1007/s40436-022-00393-2

Bimbi, A., Kawabata, M., Tsunekawa, T., & Sasahara, H. (2024). Rotary tig waam particle simulation [Paper No. GS07-14]. *Proceedings of ICPE2024: The 20th International Conference on Precision Engineering*.

Bimbi, A., Kawabata, M., Tsunekawa, T., Sasahara, H., & Campatelli, G. (2024). Influence of electrode rotation speed on geometry and internal structure of weld beads in rotary tig wire-arc-directed energy deposition. *The International Journal of Advanced Manufacturing Technology*. https://doi.org/10.1007/s00170-024-14699-x

Bonaccorso, F., Cantelli, L., & Muscato, G. (2011). An arc welding robot control for a shaped metal deposition plant: Modular software interface and sensors. *IEEE Transactions on Industrial Electronics*, *58*(8), 3126–3132. https://doi.org/10.1109/TIE.2011.2114311

Campatelli, G., Montevecchi, F., Venturini, G., Ingarao, G., & Priarone, P. C. (2020). Integrated waam-subtractive versus pure subtractive manufacturing approaches: An energy efficiency comparison. *International Journal of Precision Engineering and Manufacturing - Green Technology*, *7*(1), 1–11. https://doi.org/10.1007/s40684-019-00071-y

Carvalho, G. H. S. F. L., Venturini, G., Campatelli, G., & Galvanetto, E. (2023). Development of optimal deposition strategies for cladding of inconel 625. *Surface and Coatings Technology*, *453*, 129128. https://doi.org/10.1016/j.surfcoat.2022.129128

Cheepu, M., Lee, C. I., & Cho, S. M. (2020). Microstructural characteristics of wire arc additive manufacturing with inconel 625 by super-tig welding. *Transactions of the Indian Institute of Metals*, *73*(6), 1475–1479. https://doi.org/10.1007/s12666-020-01915-x

Chen, C., He, H., Zhou, J., Lian, G., Huang, X., & Feng, M. (2022). Recursive multi-bead overlapping model for robotic waam. *Journal of Manufacturing Processes*, *84*, 886–901. https://doi.org/10.1016/j.jmapro.2022.10.042

Dai, H., Shen, X., & Wang, H. (2018a). The influence of tig-arc physical characteristics on the penetration and weld width under different ar and he supply conditions. *Results in Physics*, *9*, 1120–1126. https://doi.org/10.1016/j.rinp.2018.04.030

Dai, H., Shen, X., & Wang, H. (2018b). Study on arc pressure of tig welding under ar-ar and ar-he supply. *Results in Physics*, *10*, 917–922. https://doi.org/10.1016/j.rinp.2018.08.015

Ding, D., Pan, Z., Cuiuri, D., & Li, H. (2015). A multi-bead overlapping model for robotic wire and arc additive manufacturing (waam). *Robotics and Computer-Integrated Manufacturing*, *31*, 101–110. https://doi.org/10.1016/j.rcim.2014.08.008

Han, Q., Li, X., Dong, M., & Zhang, G. (2021). Enhanced curve-fitting model for twin-electrode gta-based additive manufacturing. *The International Journal of Advanced Manufacturing Technology*, *116*, 1–17. https://doi.org/10.1007/s00170-021-07501-9

Huang, S. H., Liu, P., Mokasdar, A., & Hou, L. (2013). Additive manufacturing and its societal impact: A literature review. *The International Journal of Advanced Manufacturing Technology*, *67*, 1191–1203. https://doi.org/10.1007/s00170-012-4558-5

Huang, W., Ma, N., Wang, Q., Hiraoka, K., Komen, H., Shao, C., Lu, F., & Kano, S. (2024). Interpass temperature strategies for compressive residual stresses in cladding low-transformation-temperature material 16cr8ni via wire arc additive manufacturing. *International Communications in Heat and Mass Transfer*, *157*, 107777. https://doi.org/10.1016/j.icheatmasstransfer.2024.107777

Karim, M. A., Jadhav, S., Kannan, R., Pierce, D., Lee, Y., Nandwana, P., & Kim, D. B. (2024). Investigating stainless steel/aluminum bimetallic structures fabricated by cold metal

transfer (cmt)-based wire-arc directed energy deposition. *Additive Manufacturing*, *81*, 104015. https://doi.org/10.1016/j.addma.2024.104015

Kawabata, M., Sasaki, T., Wada, K., Kanemaru, S., Nomura, Y., & Sasahara, H. (2024a). Effect of arc length on deposition characteristics in rotary tungsten inert gas (tig) torch. *Journal of Advanced Mechanical Design, Systems and Manufacturing*, *18*(4). https://doi.org/10.1299/jamdsm.2024jamdsm0047

Kawabata, M., Sasaki, T., Wada, K., Kanemaru, S., Nomura, Y., & Sasahara, H. (2024b). Welding torch with coaxial wire feed and rotating electrode for wire-arc directed energy deposition. *Additive Manufacturing*, *84*, 104106. https://doi.org/10.1016/j.addma.2024.104106

Li, Y., Su, C., & Zhu, J. (2022). Comprehensive review of wire arc additive manufacturing: Hardware system, physical process, monitoring, property characterization, application and future prospects. *Results in Engineering*, *13*, 100330. https://doi.org/10.1016/j.rineng.2021.100330

Li, Y., Sun, Y., Han, Q., Zhang, G., & Horvath, I. (2018). Enhanced beads overlapping model for wire and arc additive manufacturing of multi-layer multi-bead metallic parts. *Journal of Materials Processing Technology*, *252*, 838–848. https://doi.org/10.1016/j.jmatprotec.2017.10.017

Nahmany, M., & Aghion, E. (2025). Review of the latest welding technologies for metallic components produced by additive manufacturing. *Journal of Materials Engineering and Performance*. https://doi.org/10.1007/s11665-025-12472-z

Pratheesh-Kumar, S., Elangovan, S., Mohanraj, R., & Ramakrishna, J. R. (2021). Review on the evolution and technology of state-of-the-art metal additive manufacturing processes. *Materials Today: Proceedings*, *46*, 7907–7920. https://doi.org/10.1016/j.matpr.2021.02.567

Sahoo, A., & Tripathy, S. (2019). Development in plasma arc welding process: A review. *Materials Today: Proceedings*, *41*, 363–368. https://doi.org/10.1016/j.matpr.2020.09.562

Sarkar, R., Chen, B., Fitzpatrick, M. E., Fabijanic, D., & Hilditch, T. (2022). Additive manufacturing-based repair of in718 superalloy and high-cycle fatigue assessment of the joint. *Additive Manufacturing*, *60*, 103276. https://doi.org/10.1016/j.addma.2022.103276

Selvi, S., Vishvaksenan, A., & Rajasekar, E. (2018). Cold metal transfer (cmt) technology—an overview. *Defence Technology*, *14*(1), 28–44. https://doi.org/10.1016/j.dt.2017.08.002

Shah, A., Aliyev, R., Zeidler, H., & Krinke, S. (2023). A review of the recent developments and challenges in wire arc additive manufacturing (waam) process. *Journal of Manufacturing and Materials Processing*, *7*(3), 97. https://doi.org/10.3390/jmmp7030097

Singh, S., Kumar, V., Kumar, S., & Kumar, A. (2022). Variant of mig welding of similar and dissimilar metals: A review. *Materials Today: Proceedings*, 3550–3555. https://doi.org/10.1016/j.matpr.2021.11.287

Tang, P., Zhao, X., Shi, H., Hu, B., Ding, J., Yang, B., & Xu, W. (2024). A review of multi-axis additive manufacturing: Potential, opportunity and challenge. *Additive Manufacturing*, *83*, 104075. https://doi.org/10.1016/j.addma.2024.104075

Ullah-Khan, A., Chatterjee, S., & Madhukar, Y. K. (2024).). tig assisted surface finish enhancement in mig-based wire arc additive manufacturing. *Manufacturing Letters*, *40*, 26–30. https://doi.org/10.1016/j.mfglet.2024.01.004

Vafadar, A., Guzzomi, F., Rassau, A., & Hayward, K. (2021). Advances in metal additive manufacturing: A review of common processes, industrial applications, and current challenges. *Applied Sciences*, *11*(3). https://doi.org/10.3390/app11031213

Wang, X., Wang, A., & Li, Y. (2020a). An online surface height measurement method for gtaw-based additive manufacturing. *Welding in the World*, *64*(1), 11–20. https://doi.org/10.1007/s40194-019-00813-1

Wang, X., Wang, A., & Li, Y. (2020b). Study on the deposition accuracy of omni-directional gtaw-based additive manufacturing. *Journal of Materials Processing Technology*, *282*, 116649. https://doi.org/10.1016/j.jmatprotec.2020.116649

Wu, B., Pan, Z., Ding, D., Cuiuri, D., Li, H., Xu, J., & Norrish, J. (2018). A review of the wire arc additive manufacturing of metals: Properties, defects and quality improvement. *Journal of Manufacturing Processes*, *35*, 127–139. https://doi.org/10.1016/j.jmapro.2018.08.001

Xiong, J., Zhu, B., Chen, H., & Zheng, S. (2020). Peak elimination of cross structures in wire and arc additive manufacturing using closed-loop control. *Journal of Manufacturing Processes*, *58*, 368–376. https://doi.org/10.1016/j.jmapro.2020.08.030

Xu, R., Li, R., Yuan, T., Yu, C., Wang, M., & Zhu, H. (2024). Microstructure, mechanical properties and deformation behavior of laser additively repaired 5083 and 6061 al alloys utilizing almgsczr powders. *Additive Manufacturing*, *95*, 104526. https://doi.org/10.1016/j.addma.2024.104526

Yin, S., Cavaliere, P., Aldwell, B., Jenkins, R., Liao, H., Li, W., & Lupoi, R. (2018). Cold spray additive manufacturing and repair: Fundamentals and applications. *Additive Manufacturing*, *21*, 628–650. https://doi.org/10.1016/j.addma.2018.04.017

Zhang, H., Li, R., Liu, J., Wang, K., Weijian, Q., Shi, L., Lei, L., He, W., & Wu, S. (2024). State-of-art review on the process-structure-properties-performance linkage in wire arc additive manufacturing. *Virtual and Physical Prototyping*, *19*(1), e2390495. https://doi.org/10.1080/17452759.2024.2390495